Dislocations and a domains coupling in PbTiO3 thin films

Long Cheng, Heng Zhang, Ran Xu, Kevin Co, Nicolas Guiblin, Mojca Otoničar, Charles Paillard, Yujia Wang, Brahim Dkhil

Dislocations and *a* domains coupling in $PbTiO_3$ thin films

Long Cheng,[a*] Heng Zhang,[b,c] Ran Xu,[a] Kevin Co,[a] Nicolas Guiblin,[a] Mojca Otoničar,[d] Charles Paillard,[a,e] Yujia Wang,[b] Brahim Dkhil [a]

[a] Université Paris-Saclay, CentraleSupélec, CNRS, Laboratoire SPMS, 91190, Gif-sur-Yvette, France.

[b] Shenyang National Laboratory for Materials Science, Institute of Metal Research, Chinese Academy of Sciences, Wenhua Road 72, Shenyang 110016, China

[c] School of Materials Science and Engineering, University of Science and Technology of China, Wenhua Road 72, Shenyang 110016, China

[d] Jožef Stefan Institute and Jožef Stefan Postgraduate School, Jamova 39, 1000, Ljubljana, Slovenia

[e] Physics Department, University of Arkansas, Fayetteville, Arkansas 72701, USA

* Corresponding author. E-mail address: long.cheng@centralesupelec.fr (L. Cheng).

L. Cheng and H. Zhang contributed equally to this work.

Abstract

The interaction of domain structure and defects in ferroelectric thin films has been studied for decades. However, the role of dislocations and thermal stability of microstructures are still poorly studied. By combining transmission electron microscopy, X-ray diffraction experiments and phase-field simulations, we show that dislocation pairs induced by post-annealing above 550 °C provide a stress field stabilizing *a* domains in 30 nm thick tetragonal $PbTiO_3$ films on $SrTiO_3$ substrate, initially exhibiting pure *c* domains. Based on phase-field simulations we further discuss the effects of single dislocations and dislocation pairs on the nucleation of *a*-domains and the occurrence of non-ferroelastic 180° domains. Dislocations, and the possibility to tune them using an appropriate thermal annealing process, offer a path for modulating the domains and domain wall states and thus the physical properties of ferroelectric films.

Keywords: ferroelectric, thin film, domain structure, dislocations

Ferroelectric thin films have become promising for the creation of non-volatile memories, energy harvesting and MEMS devices. [1–3] Understanding and controlling the domain structure of ferroelectric thin films is vital to realize large-scale applications.[4–7] Generally, the switching and rearrangement of domains is active well below the film growth temperature.[8,9] Intrinsic factors such as substrate clamping (due to mismatch of the unit cell parameters) and depolarizing field (which increases when the sample thickness decreases) determine to a large extent the stable room-temperature ferroelectric domain configuration.[10] However, it was found experimentally that growth parameters such as growth temperature,[11] oxygen pressure,[12] annealing rate,[13] and quenching[14] can affect the domain structures of ferroelectric films, indicating that other factors such as defects may play a key role as well.[15]

Indeed, defects such as vacancies[11], element-enriched phases[12] and dislocations[7] inevitably appear in the film and can affect the formation of domains. It is for instance well-known that point defects accumulate and pin the ferroelectric domain walls, i.e. boundaries separating two adjacent ferroelectric domains having different polarization directions.[16,17] These point defects can also form local defect dipoles which couple to the growth direction to produce polarization gradient.[15] Defects with higher dimensionality, such as dislocations (typical linear defects), have been studied for decades in epitaxial thin films.[18,19] It was proposed that interfacial dislocations lead to the preferential formation of *a* domains (with in-plane polarization, in contrast to *c* domains with out-of-plane polarization), relaxing the elastic energy due to misfit strain. In fact, just as point defects and domain wall pin each other, the interaction between dislocations and *a*-domain can slow down the motion of *a* domains, inducing large local polarization inhomogeneity, and thus destroy the properties of devices made by ferroelectric films.[20–23] Yet, the interaction of dislocations with ferroelectric domain walls also offers fantastic opportunities for improved device performances, as recently reported.[24] Indeed, depending on the dislocation type, it has been shown that dislocation-domain wall interactions can generate extraordinary and stable large-signal dielectric permittivity and piezoelectric coefficient[24,25].

Most studies of the domain-dislocation interaction in ferroelectric films have been carried out at room temperature. With the increasing demand for ferroelectric devices operating at higher temperatures,[26] it is critical to go beyond the room temperature features.

We thus need to study the thermal stability of domain structures and the interaction between domains and dislocations at elevated temperatures. It is worth mentioning that while thermal annealing appears as a random process, recent works[15] have demonstrated that, in addition to the well-established electrostatic and mechanical boundary conditions, the growth temperature is efficient to modulate defects and consequently offers a tool for the full control of the polarization in ferroelectric thin films through mono- to poly-domain configurations. Here, we employ annealing to modulate the domain structures of $PbTiO_3$ (PTO) thin films. We report that *a* domains can be generated in 30 nm thick PTO films deposited on (001)-oriented $SrTiO_3$ (STO) substrates when annealed at temperatures above 550 °C. Transmission electron microscopy (TEM) and temperature-dependent X-ray diffraction (XRD) allow to access the microstructure of ferroelectric PTO films. Phase-field simulations further confirm that the existence of interfacial dislocations stabilize *a* domains in PTO films.

30 nm thick PTO films were grown on single-crystal (001)-oriented STO substrates by pulsed laser deposition (PLD), using a KrF excimer laser (λ=248 nm) (see details in the **Supplementary materials**). As-grown samples were then annealed at 500 °C or 700 °C for 15 min in a separate furnace and then removed from the furnace and rapidly quenched in air. Bright-field and dark-field TEM images (see **Supplementary materials**) were acquired by Tecnai G^2 F30 microscope (FEI, USA). High-angle annular dark-field (HAADF) scanning TEM (STEM) images were recorded at 300 kV using Titan G^2 60-300 kV microscope (FEI, USA). Strain analysis was based on geometric phase analysis (GPA), carried out using Gatan Digital Micrograph software.

XRD was performed on a homemade diffractometer with a Rigaku RA-HF18 rotating anode source (50 kV, 300 mA) using Cu Kα_1 (0.15405 nm) wavelength equipped with a furnace allowing to acquire patterns from room temperature (RT) to 667°C (see **Supplementary materials**).

At room temperature, bulk PTO is ferroelectric with a tetragonal structure (space group *P*4*mm*) with lattice constants of a = b = 0.3904 nm and c = 0.4157 nm,[27] whereas the STO crystal has a cubic structure with lattice constants of a = b = c = 0.3905 nm.[28] Accordingly,[10] the pulsed laser deposited PTO thin films are epitaxially grown on (001)-oriented STO substrates and show (00l) *c* domain orientation (see **Figure S1** in Supplementary Materials) with the *c*-axis perpendicular to the substrate, resulting in an almost strain-free film.

To identify the domain structure of the PTO thin films annealed at different temperatures, namely at 500 °C and 700 °C, TEM observations were carried out. **Figure 1** shows the cross-sectional TEM dark-field images of the PTO films along the [100] direction. The as-grown film (see **Figure 1**a) shows vertical stripe domains with alternating bright and dark contrast, indicating 180° domain walls[29] (pure *c* domains, i.e., out-of-plane polarization). Because these films are grown on an insulating STO substrate, domains with opposite polarization form to reduce the depolarization field and maintain the ferroelectric state.[30] PTO films annealed at 500 °C and 700 °C are presented in **Figure 1**b and **Figure 1**c, respectively. The film annealed at 500 °C (**Figure 1**b) shows an increase in the density of 180° domain walls compared to the as-grown film (see **Figure 1**a). The Kittel's scaling law which states the domain period (or number of domain walls) is proportional to the film thickness appears to not be working here as the film thickness is fixed. This deviation can be explained by the nature of the domain walls.[31] Indeed, as one can notice in **Figure 1**b, some domain walls deviate from 180° (see blue dashed lines in **Figure 1**a&b), and might be due to some defect segregation favoring non-ferroelastic 180° charged domain walls[32] altering the depolarizing field.[33-35] After annealing at higher temperature, 700 °C (see **Figure 1**c), 45° inclined stripes crossing the entire film emerged. They attest of the presence of ferroelastic 90° domain walls separating *a* and *c* domains. This observation is surprising, as the current strain conditions (almost strain-free films) do not in general favor the formation of *a*-*c* domain configurations, which are rather obtained under *tensile* strain.[13,36]

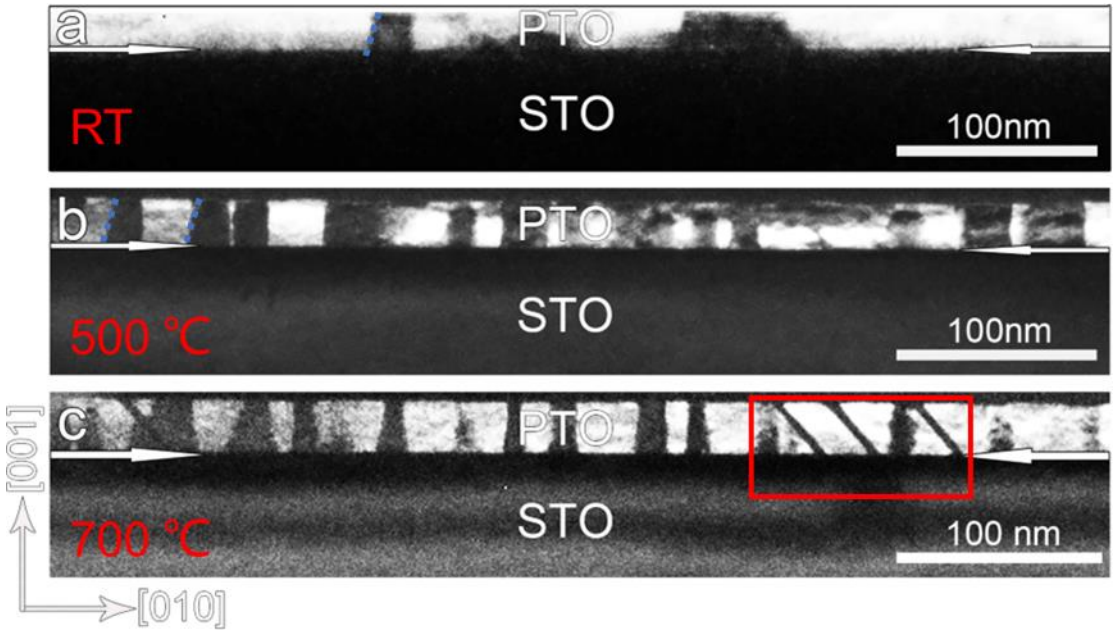

Figure 1. The cross-sectional dark-field TEM images of the 30 nm PTO films grown on (001) STO substrates: (a) as-prepared sample without heat treatment, (b) sample annealed at 500 °C, and (c) sample annealed at 700 °C. White arrows mark the interface. Blue dashed lines show domain walls deviating from 180°. Red rectangle highlights the *a* domains, oriented at 45° to the substrate, representing the *a*–*c* domain structure with 90° domain walls separating the *a* and *c* domains.

To further reveal the origin of these unexpected *a* domains, HAADF-STEM is employed on the 700 ℃-annealed sample (see **Figure 2**). Interestingly, near the intersection of the *a* domain with the PTO/STO interface, a pair of dislocations was identified; see in Figure 2b an enlarged view of the area marked by a white dashed square in **Figure 2**a. No dislocation pairs were spotted in the *c* domain configurations, nor in the as-grown and 500 °C-annealed films. Two types of mutually perpendicular edge dislocations form a dislocation pair near the interface. These two types of edge dislocations are named as C-type and G-type dislocations according to their semi-atomic planes and migration modes (C-type, climbing dislocation; G-type, gliding dislocation). The Burgers vector of the C-type dislocation is **b**=a[0$\bar{1}$0] corresponding to the dislocation at the interface; the Burgers vector of the G-type dislocation is **b**=a[001] corresponding to the edge dislocation inside the film. As a result, the extra half-atomic plane

at the interface (C-type dislocation) may generate a local normal *tensile* stress here. Note that while they are also possible to occur, we do not observe any <110>-like dislocations in the investigated atomic areas as they are believed to decompose into two partial dislocations to form a pinning effect on the *a* domain[29,37]. **Figure 2**c presents the in-plane strain (ε_{xx}) obtained from the GPA performed on the area in **Figure 2**a. The red area in the **Figure 2**c corresponds to the position of the *a* domain. **Figure 2**c reveals that the strain in the *a* domain (red lamellae) is about 6%, and the strain at the core of the dislocation pair (black and white spot indicated by arrows in **Figure 2**c) is larger than that at the *a* domain. **Figure 2**d shows the lattice rotation (R_y) where the *a* domain (green lamellae) corresponds to about 0° while the *c* domain (red region) to about 3°, that is linked to the *c/a* ratio and in agreement with previous reports.[36,40] (see arrows in **Figure 2**d). This result indicates that the dislocation pair and the *a* domain exhibit a pinning effect between each other, making them more likely to be retained.

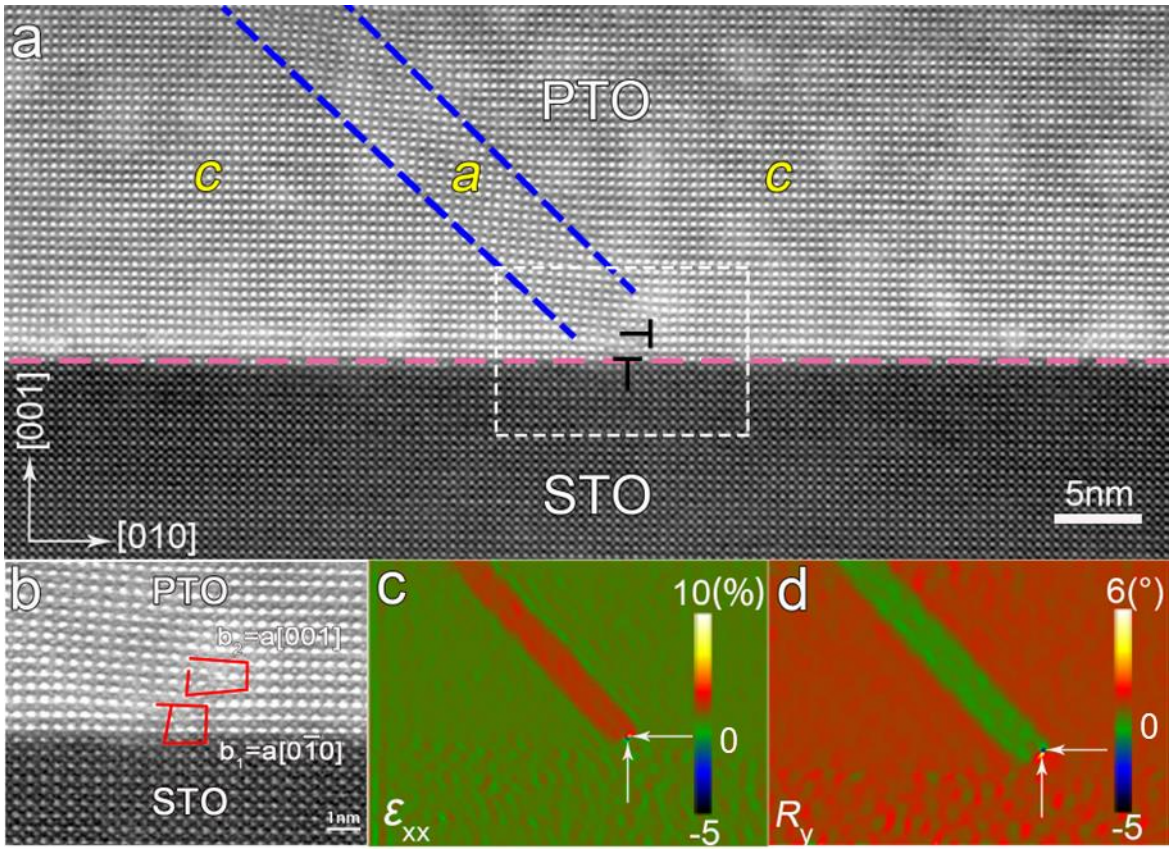

Figure 2. High-resolution HAADF-STEM images and related GPA results. (a) HAADF image of one *a* domain separated from the *c* domains by 90° domain walls, marked by blue dashed

lines. The cores of two dislocations are labeled by “T”. Pink dashed line marks the interface. (b) Enlarged view of the area shown by the white dashed square in (a). Red lines mark the dislocations with different Burgers vectors: **b**=a[$0\bar{1}0$] for dislocation at the interface; **b**=a[001] for edge dislocation inside the film. (c) In-plane strain (ε_{xx}) corresponding to (a). The red area corresponds to the position of the *a* domain. (d) Lattice rotation (R_y) with *a* domain taken as zero rotation. White arrows mark the position of the dislocation pair.

To further reveal the formation of *a* domains, the annealing process on a virgin $PbTiO_3$ thin film from 27 °C to 667 °C was investigated using high temperature XRD. XRD patterns of the (200) Bragg peak at different temperatures are shown in **Figures S2** and **S3** for heating and cooling respectively. **Figure 3**a shows the *c*-axis (out-of-plane) lattice constants of PTO and lattice constants of STO on heating and cooling processes. As one can see, the *c*-parameter evolves monotonously with the temperature, and there is no indication of any phase transition up to 667 °C on both heating and cooling regimes, in good agreement with previous reports.[30,38] Indeed, the critical Curie temperature in classical ferroelectric films such as $PbTiO_3$ is known to be strongly enhanced because of electromechanical boundary conditions and finite size effects leading to the renormalization of the Landau coefficients and stabilization of ferroelectric phases[39]. The full width at half maximum (FWHM) values of diffraction peaks during heating and cooling regimes are shown in **Figure 3**b. It is observed that the FWHM starts to strongly increase during the heating process above about 550 °C (see **Figure 3**b). On cooling, the FWHM decreases and reaches a plateau at about 400 °C, and the value of the plateau on cooling is higher (~0.61°) than that on heating (~0.58°). The broadening of the FWHM has been related to the heterogeneous strain coming from defects.[26, 27] It is thus likely that some defects (both point defects and dislocations) are generated above a critical temperature that is ~550 °C, and some are kept and/or reorganized (e.g., segregation of point defects at domain walls) on cooling (below ~400 °C) when coming back to room temperature. These defects and, most likely, the dislocations observed in **Figure 2** only in the sample annealed at 700 °C, can thus create strain states that favor the formation of *a* domains. Coupling between *a* domains and dislocation pairs might thus occur through this annealing process at

temperatures above 550˚C. This phenomenon can be used for tuning the polarization response of the PTO film.[15]

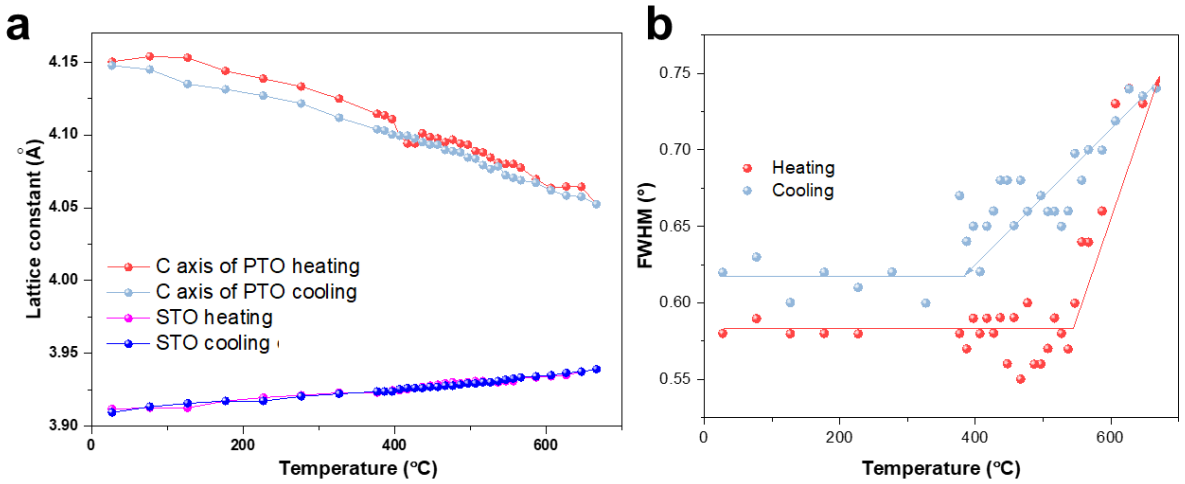

Figure 3. The results of XRD with different temperatures. (a) The temperature dependence of *c*-axis lattice constants of PTO and lattice constants of STO on heating process and cooling process. (b) FWHM values of (002) diffraction peak during heating process and cooling process. Straight lines are guides for the eyes.

To further clarify the coupling between the domain structures and the pair of dislocations appearing at the interface to help *a* domains to form, 2D phase-field simulations were carried out (see details in the **Supplementary materials**). We constructed four models of 30 nm thick PTO thin films on STO substrates: the first one is an ideal film without dislocation pairs, and the second one is a film with periodic dislocation pairs. The dislocation pair consists of a C-type dislocation with **b**=a[$\bar{1}$00], **n** =(1,0,0), and a G-type dislocation with **b**=a[001] and **n**=(1,0,0). This dislocation system is comparable to what we observe in **Figure 2**. The third and fourth models are films with periodic C-type and G-type dislocations, respectively. The period of the dislocation pairs and single dislocations is 50 nm, which is much larger than the distance between the two adjacent dislocations in a pair (5 nm). **Figure 4** illustrates the domain structures at 25 °C obtained by phase-field simulation for the four models we considered. In the absence of dislocations, the equilibrium domain structures consist solely of pure *c* domains within the film, as depicted in **Figure 4**a, in agreement with our experimental observations

(**Figure 1**a-b). However, when the interfacial dislocation pairs are added, *a* domains are induced near the dislocation pairs (see **Figure 4**b), also in agreement with TEM observations (**Figure 2**). We further calculate the cases with only C-type or G-type dislocations at the interface to disentangle the effects of the dislocation pairs. Remarkably, we can still observe the formation of *a* domains when only C-type dislocations are added (see **Figure 4**c). However, when only G-type dislocations are considered, *a* domains are not formed at room temperature, and only subtle polarization changes and curved non-ferroelastic 180° domain walls, resembling those observed in **Figure 2**b, are observed near the core of G-type dislocations (see **Figure 4**d). These calculations therefore show that in addition to point defects,[32,33] dislocations can also alter the strain state within 180° domain walls in ferroelectric thin films. The introduction of dislocation strain/stress fields, especially of C-type dislocations, thus changes the elastic energy of the system and promotes stabilization of 90° *a*-*c* domain structures. Our calculations and their agreement with our experimental observations demonstrate there is a clear coupling between the *a* domains and dislocations.

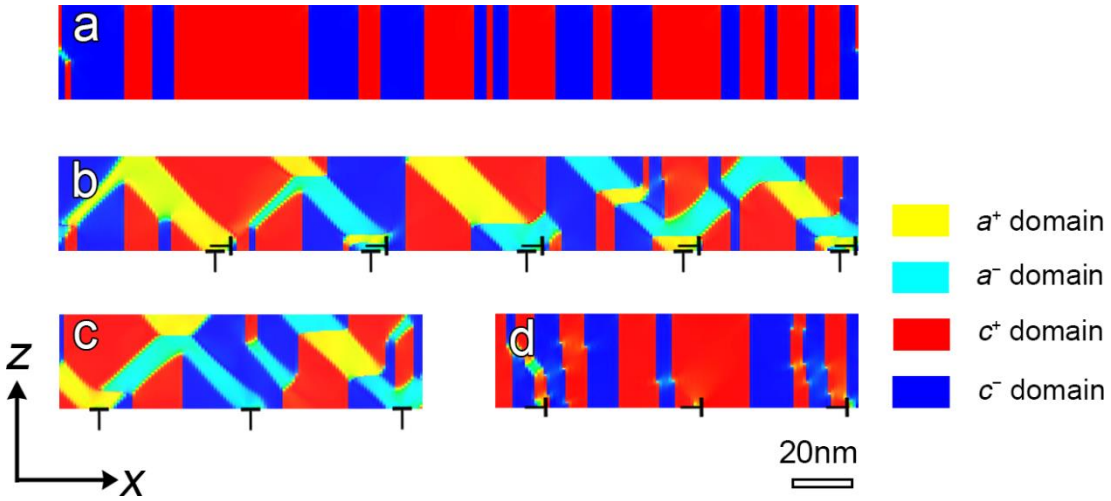

Figure 4. Domain structures of 30 nm PTO thin films grown on STO substrate at 25 °C obtained by 2D phase-field simulations. (a) The ideal film without dislocation pair. (b) The film with periodic dislocation pairs. (c) The film with periodic C-type dislocations, and (d) periodic G-type dislocations. The dislocation period is taken to be 50 nm.

By combining experiments and simulations, we demonstrate that dislocation pairs couple to *a*

domains and favor their stabilization. Two possibilities for the nucleation of *a* domains can be considered. The first one relies on the formation of dislocations induced by the chaotic arrangement of some atoms at the interface/inside the substrate or volatility of lead and oxygen elements due to high temperature. As the temperature rises, some dislocations overcome the relatively high Peierls barrier in the perovskite film,[41,42] gliding to the interface. The lattice distortion around the dislocations provides a stress field, which helps to stabilize *a* domains. The dislocations, like point defects, also contribute to non-ferroelastic 180° domain walls. A second scenario is that prior to the Curie temperature, as the temperature increases, the *c/a* ratio decreases and since their strain states become closer to each other, some of the *c* domains are converted to *a* domains by the depolarization field. The generated *a* domains lead to a local increase in strain. Dislocation pairs can thus form around *a* domains to release strain, leading to the coexistence of *a* domains and dislocation pairs at the interface as well as *c* domains with domain walls deviating from 180°. In either cases, this phenomenon occurs above 550 °C, which corresponds to the FWHM jump in **Figure 3**b. The appearance of the dislocations is thus a thermally activated process.

This phenomenon takes place above a critical temperature in epitaxial PTO films. The dislocation pairs go hand in hand with *a* domains to release the additional stress, and therefore the strain coupling between *a* domains and dislocation pairs provides a way for stabilizing 90° domain walls.[37] Earlier works[37,38,43] have also pointed in that direction, without clear understanding of thermal effects at the time.

In summary, by using aberration-corrected STEM, high-temperature XRD and phase-field simulations, the link between *a* domains and dislocation pairs in PTO films is studied. It is found that the 90° domain walls are favored by the dislocations and can be controlled by heat treatment in the PTO film above a critical temperature. By phase-field simulations, we found that the single dislocations (C- type) can also solely induce *a* domains. However, based on our experimental observations, it is believed that dislocation pairs are more favorable for the retention of *a* domains by playing a pinning role. Our work provides a reference for

understanding the mechanism of thermal strain relaxation and the interaction of dislocations with *a* domains in ferroelectric thin films.

See supplementary materials for XRD patterns of PTO film grown on STO (001) substrate in Figure S1, XRD patterns of PTO film grown on STO (001) substrate during heating process in Figure S2, and on cooling process in Figure S3.

ACKNOWLEDGMENTS

The authors are grateful for the support from professor X. L. Ma (now at Songshan Lake Materials Laboratory), professor Y. L. Tang, at Shenyang National Laboratory for Materials Science, Institute of Metal Research, Chinese Academy of Science, and Y. P. Feng, W. R. Geng (now at Songshan Lake Materials Laboratory) for experimental assistance with STEM. We are grateful to Prof. J. Y. Li at Southern University of Science and Technology and Dr. C. H. Lei at Saint Louis University for the development of the phase-field code. Long Cheng and Ran Xu's work is also supported by the China Scholarship Council. The authors also acknowledge support from the Agence Nationale de la Recherche (ANR) through THz-MUFINS (ANR-21-CE42-0030), TATOO (ANR-21-CE09-0033-02) and SUPERSPIN (ANR-21-CE24-0032) projects, PHC Slovenian-French Proteus mobility grant (BI-FR/21-22-PROTEUS-004) and Slovenian Research Agency ARRS through program P2-0105 and project J2-2508, the National Natural Science Foundation of China (52122101), Shenyang National Laboratory for Materials Science (L2019F13), the Youth Innovation Promotion Association CAS (2021187).

AUTHOR'S CONTRIBUTIONS

L. C, and H. Z conceived the idea of the work and designed the project. L. C fabricated and characterized the thin films. H. Z, K. C and R. X did the phase-field simulations. L. C and H. Z wrote the draft of the manuscript. N. G did the in-situ XRD experiments. M. O, C. P and B. D revised the manuscript. All authors contributed to the discussion of the work.

DATA AVALAIBILITY

The data that support the findings of this study are available within the article [and its

supplementary material].

References

[1]M. Si, A. K Saha, S. Gao, G. Qiu, J. Qin, Y. Duan, J. Jian, C. Niu, H. Wang, W. Wu, S. K. Gupta, P. D. Ye., Nat Electron **2**, 580 (2019).

[2]Y. Bai, H. Jantunen, and J. Juuti, Adv. Mater. **30**, 1707271 (2018).

[3]P. Yudin, K. Shapovalov, T. Sluka, J. Peräntie, H. Jantunen, A. Dejneka, and M. Tyunina, Sci Rep **11**, 1899 (2021).

[4]V. Nagarajan, A. Roytburd, A. Stanishevsky, S. Prasertchoung, T. Zhao, L. Chen, J. Melngailis, O. Auciello, and R. Ramesh, Nat Mater **2**, 43 (2003).

[5]N. A. Pertsev and A. G. Zembilgotov, J. Appl. Phys. **78**, 6170 (1995).

[6]C. S. Ganpule, V. Nagarajan, H. Li, A. S. Ogale, D. E. Steinhauer, S. Aggarwal, E. Williams, R. Ramesh, and P. De Wolf, Appl. Phys. Lett. **77**, 292 (2000).

[7]P. Gao, C. T. Nelson, J. R. Jokisaari, S. H. Baek, C. W. Bark, Y. Zhang, E. Wang, D. G. Schlom, C.-B. Eom, and X. Pan, Nat Commun **2**, 591 (2011).

[8]N. A. Pertsev and A. G. Zembilgotov, J. Appl. Phys. **80**, 6401 (1998).

[9]K. S. Lee, Y. K. Kim, S. Baik, J. Kim, and I. S. Jung, Appl. Phys. Lett. **79**, 2444 (2001).

[10]M. Dawber, C. Lichtensteiger, J. M. Triscone, Phase Transit, **81**, 623 (2008)

[11]J. Moon, J. A. Kerchner, J. LeBleu, A. A. Morrone, and J. H. Adair, J. Am. Ceram. Soc. **80**, 2613 (2005).

[12]L. Cheng, Y. Tang, Y. Zhu, and X. Ma, J. Cryst. Growth. **20**, 5967 (2020).

[13]J. Y. Ma, Y. Zhu, Y. Tang, M. Han, Y. Wang, N. Zhang, M. Zou, Y. Feng, W. Geng, and X. Ma, RSC Adv. **9**, 13981 (2019).

[14]Y. Nahas, S. Prokhorenko, J. Fischer, B. Xu, C. Carrétéro, S. Prosandeev, M. Bibes, S. Fusil, B. Dkhil, V. Garcia and L. Bellaiche, Nature **577**, 47 (2020)

[15]C. Weymann, C. Lichtensteiger, S. Fernandez-Pena, A. B. Naden, L. R. Dedon, L. W. Martin, J. M. Triscone, P. Paruch, Adv. Electron. Mater. **6**, 2000852 (2020)

[16]A. Chandrasekaran, D. Damjanovic, N. Setter, and N. Marzari, Phys. Rev. B **88**, 214116 (2013).

[17]C. Paillard, G. Geneste, L. Bellaiche, and B. Dkhil, J. Phys. Condens. Matter **29**, 485707 (2017).

[18]M. W. Chu, I. Szafraniak, R. Scholz, C. Harnagea, D. Hesse, M. Alexe, and U. Gösele, Nat Mater **3**, 87 (2004).

[19]S. Y. Hu, Y. L. Li, and L. Q. Chen, J. Appl. Phys. **94**, 2542 (2003).

[20]Y. L. Tang, Y. L. Zhu, Y. Liu, Y. J. Wang, and X. L. Ma, Nat Commun **8**, 15994 (2017).

[21]Y. Zheng, B. Wang, and C. H. Woo, J. Phys. Chem. Solids. **55**, 1661 (2007).

[22]H. H. Wu, J. Wang, S. G. Cao, and T. Y. Zhang, Appl. Phys. Lett. **102**, 232904 (2013).

[23]T. Shimada, T. Xu, Y. Araki, J. Wang, and T. Kitamura, Nano Lett. **17**, 2674 (2017).

[24]F. Zhuo, X. Zhou, S. Gao, M. Höfling, F. Dietrich, P. B. Groszewicz, L. Fulanović, P. Breckner, A. Wohninsland, B.-X. Xu, H. J. Kleebe, X. Tan, J. Koruza, D. Damjanovic, and J. Rödel, Nat. Commun. **13**, 6676 (2022)

[25]M. Höfling, X. Zhou, L. M. Riemer, E. Bruder, B. Liu, L. Zhou, P. B. Groszewicz, F. Zhuo,

B. Xu, K. Durst, X. Tan, D. Damjanovic, J. Koruza, and J. Rödel, Science **371**, 964–971 (2021).
[26]U. De, K. R. Sahu, and A. De, SSP **232**, 235 (2015).
[27]T. Morita and A. Cho, Integr. Ferroelectr. **64**, 247 (2004).
[28]J. He, R. F. Klie, G. Logvenov, I. Bozovic, and Y. Zhu, J. Appl. Phys. **101**, 073906 (2007).
[29]K. Aoyagi, T. Kiguchi, Y. Ehara, T. Yamada, H. Funakubo, and T. J. Konno, Sci. Technol. Adv. Mater. **12**, 034403 (2011).
[30]S. K. Streiffer, J. A. Eastman, D. D. Fong, Carol Thompson, A. Munkholm, M. V. Ramana Murty, O. Auciello, G. R. Bai, and G. B. Stephenson, Phys. Rev. Lett. **89**, 067601 (2002).
[31]C. M. Teodorescu, Results Phys. **46**, 106287 (2023)
[32]K. Shapovalov, P. V. Yudin, A. K. Tagantsev, E. A. Eliseev, A. N. Morozovska, and N. Setter, Phys. Rev. Lett. **113**, 207601 (2014).
[33]C. Weymann, S. Cherifi-Hertel, C. Lichtensteiger, I. Gaponenko, K. D. Dorkenoo, A. B. Naden, and P. Paruch, Phys. Rev. B. **106**, L241404 (2022)
[34]G. De Luca, M. D. Rossell, J. Schaab, N. Viart, M. Fiebig, and M. Trassin, Adv. Mater. **29**, 1605145 (2017).
[35]Y. X. Jiang, Y. J. Wang, D. Chen, Y. L. Zhu, and X. L. Ma, J. Appl. Phys. **122**, 054101 (2017)
[36]S. Li, Y. L. Zhu, Y. L. Tang, Y. Liu, S. R. Zhang, Y. J. Wang, and X. L. Ma, Acta Materialia. **131**, 123 (2017).
[37]D. Su, Q. Meng, C. A. F. Vaz, M. G. Han, Y. Segal, F. J. Walker, M. Sawicki, C. Broadbridge, and C. H. Ahn, Appl. Phys. Lett. **99**, 102902 (2011)
[38]P. E. Janolin, F. Le Marrec, J. Chevreul, and B. Dkhil, Appl. Phys. Lett. **90**, 192910 (2007)
[39]N. A. Pertsev, A. G. Zembilgotov, and A. K. Tagantsev, Phys. Rev. Lett. 80, 1988 (1998)
[40]Y. Liu, Y.-L. Tang, Y.-L. Zhu, W.-Y. Wang, and X.-L. Ma, Adv. Mater. Interfaces **3**, 1600342 (2016)
[41]S. Stemmer, S. K. Streiffer, F. Ernst, and M. Rühle, Physica Status Solidi (a) **147**, 135 (1995).
[42]Y. L. Tang, Y. L. Zhu, H. Meng, Y. Q. Zhang, and X. L. Ma, Acta Materialia **60**, 5975 (2012).
[43]Y. P. Feng, R. J. Jiang, Y. L. Zhu, Y. L. Tang, Y. J. Wang, M. J. Zou, W. R. Geng and X. L. Ma, RSC Adv. **12**, 20423 (2022)